Soft Matter

Effects of Receptor Properties on Particle Internalization through Receptor-mediated Endocytosis

Journal:	*Soft Matter*
Manuscript ID	SM-ART-02-2023-000149.R1
Article Type:	Paper
Date Submitted by the Author:	23-Jun-2023
Complete List of Authors:	Billah, Md Muhtasim; Washington State University, School of Mechanical and Materials Engineering Deng, Hua; Washington State University, Mechanical and Materials Engineering Dutta, Prashanta; Washington State University, School of Mechanical and Materials Engineering Liu, Jin; Washington State University, School of Mechanical and Materials Engineering

ARTICLE

Effects of Receptor Properties on Particle Internalization through Receptor-mediated Endocytosis

Received 00th January 20xx,
Accepted 00th January 20xx

DOI: 10.1039/x0xx00000x

Md Muhtasim Billah, [a] Hua Deng, [b] Prashanta Dutta [a] and Jin Liu *[a]

Receptor-mediated endocytosis (RME) is a highly complex process taken by bioparticles, such as viruses and drug carriers, to enter cells. The discovery of both clathrin-dependent and clathrin-free pathways makes the RME process even more intriguing. Numerical models have been developed to facilitate the exploration of the process. However, the impacts from the receptor properties on RME have been less studied partially due to the oversimplifications of the receptor models. In this paper, we implement a stochastic model to systematically investigate the effects of mechanical (receptor flexure), geometrical (receptor length) and biochemical (ligand-receptor cutoff) properties of receptors, on RME with and without the existence of clathrin. Our simulation results show that that the receptor flexural rigidity plays important roles in RME with clathrin. There is a threshold beyond which particle internalization will not occur. Without clathrin, it is very difficult to have a complete endocytosis with ligand-receptor interactions alone. Shorter receptor length and longer ligand-receptor reaction cutoff promote formation of ligand-receptor bonds and facilitate particle internalization. A complete internalization can only be obtained with extremely short receptor length and long reaction cutoff. Therefore, there is most likely some additional mechanisms to drive the membrane deformation in clathrin-free RME. Our results yield important fundamental insights on RME and provide crucial guidance when correlating the simulation results with experimental observations.

Introduction

Receptor-mediated endocytosis (RME) is one of the most important endocytic pathways taken by bioparticles, such as viruses[1–3] and drug carriers,[4–6] to enter the cells. Among the endocytic pathways, RME is the most common form, and they are mostly accompanied by clathrin. Consequently, it is often interchangeably referred as the clathrin-mediated endocytosis (CME). CME is the dominant endocytic mechanism taken by cells and the CME process has been most studied and best characterized. For a long time, there was an ongoing debate about the driving force for cell membrane deformation and the apparent role of clathrin during vesicle budding.[7–10] It has been well demonstrated that clathrin is essential for creating matured vesicles through membrane budding.[7] Experiments also showed that clathrin polymerization alone was able to generate spherical buds, AP2 and other accessory proteins were required to control and enhance the efficiency of CME.[8] Binding to the corresponding ligands on a bioparticle helps stabilize the receptor molecules on cell and may facilitate AP2 recruitment which eventually leads to clathrin accumulation.[11,12] Particles, such as influenza viruses, can also enter cells through endocytosis when the formation of clathrin coats are inhibited.[13,14]. More recently, experiments have shown that ligand-coated nanoparticles can be internalized by different cells through caveolae-mediated endocytosis.[15,16] In addition to the clathrin/caveolae-mediated endocytosis, nanoparticles and other cargos such as cellular fluids, growth hormones and toxins can be internalized via clathrin/caveolae-independent endocytosis. A variety of clathrin/caveolae-independent pathways has been identified in recent years and details on the processes can be found in latest reviews.[17,18]

[a] School of Mechanical and Materials Engineering, Washington State University, Pullman, WA 99163, USA. Email: jin.liu2@wsu.edu
[b] Google, Kirkland, WA 98033, USA.

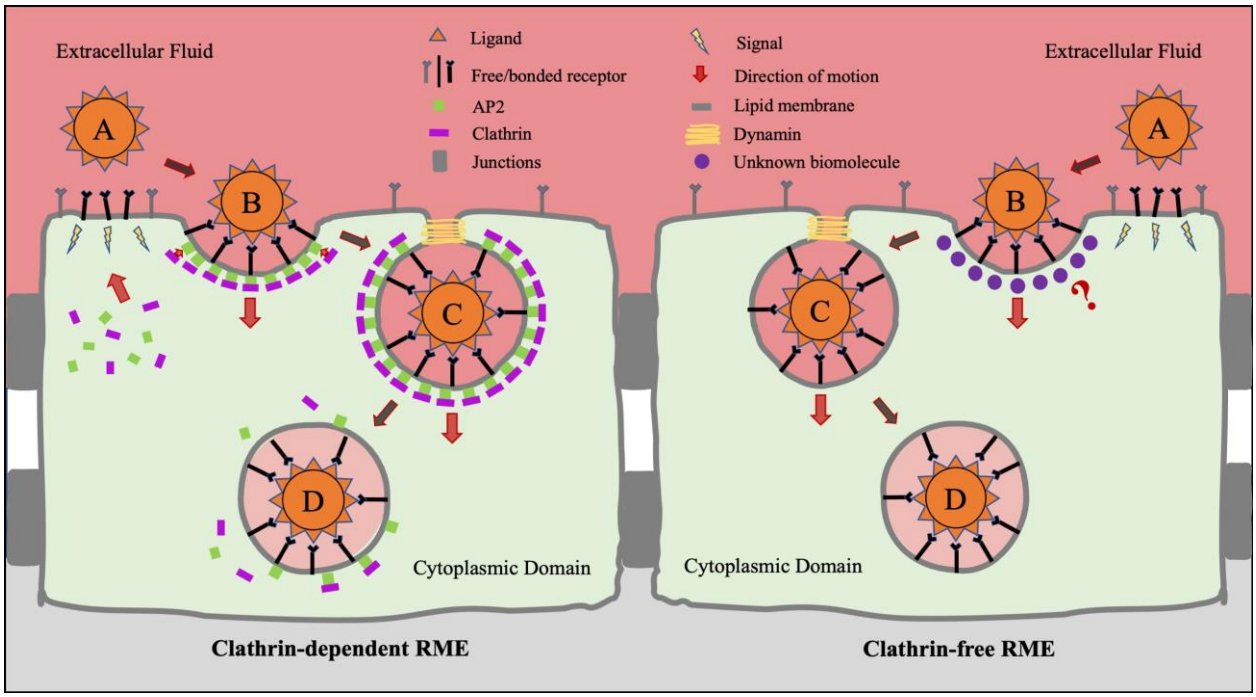

Fig. 1 Schematic of the clathrin-dependent and clathrin-free RME of ligand-coated bioparticles. For both cases, the bioparticle first attaches to the cell membrane through ligand-receptor interactions. Then, for clathrin-dependent case, a transmembrane signal triggers the assembly of clathrin and consequently, clathrin-coated pit (CCP) is formed. For clathrin-free case, particle is internalized by some other possible mechanisms. After being fully enveloped, the particle containing vesicle pinches off (scission) from the inner membrane leaflet with the help of dynamin.

As demonstrated in **Fig. 1**, RME of particles is a highly complex process that may involve many trans-membrane and peripheral membrane proteins. The overall process is dictated by collective and cooperative interplay of dynamic and multiscale events, such as particle motion, membrane deformation, receptor diffusion, as well as molecular scale protein-protein and protein-lipid interactions. The discovery of clathrin-free RME makes the process more intriguing and brings up the ambiguities regarding the functional roles of clathrin in membrane deformation. Due to its complexity and multiscale nature, experimental investigation of RME remains a challenge. Numerical studies and models have been developed to study this biological process at different levels. The models include the continuum models[19–22] and discrete models such as coarse-grained molecular dynamics (CGMD)[23–26] and dissipative particle dynamics (DPD).[27–30] Some of the models have been designed to study RME with the absence of clathrin, and demonstrated that ligand-receptor interactions were able to drive the particle internalization without clathrin.[23,24,26–28] However, the physical dimensions of the receptors have been oversimplified in most of the models. As a result, the mechanical properties of receptors, such as the flexural rigidities, are usually overlooked and there has been a wide range of ligand-receptor biochemical binding parameters employed in different models. This fact makes it difficult to directly correlate the simulation results to experimental observations.

Recently, we developed a stochastic Monte Carlo model for clathrin-mediated endocytosis of ligand-coated bioparticles. This model has been rigorously validated in our previous works[31–33] that were focused on the aspects of bioparticle internalization in regards with the particle size, shape, surface coverage (ligand density), ligand-receptor binding affinity and cellular membrane stiffness. In our model, we directly take the physical dimensions of the ligands and receptors into account. Using our model, in this work we systematically study the effects of geometrical and mechanical parameters of receptors, as well as the biochemical ligand-receptor interaction parameters, on the overall process of RME. Especially with our model we are able to delineate the functional roles of clathrin during particle internalization. In the following sections, we first briefly describe our model, then discuss the effects of receptor flexural rigidity, receptor length and ligand-receptor interaction cutoff on particle internalization with and without the clathrin. Our results show that receptor flexure plays crucial roles during ligand-coated particle internalization in RME. Moreover, the clathrin is the primary driving force, without clathrin, a complete endocytosis of particles is very unlikely through ligand-receptor interactions only.

Model and methods

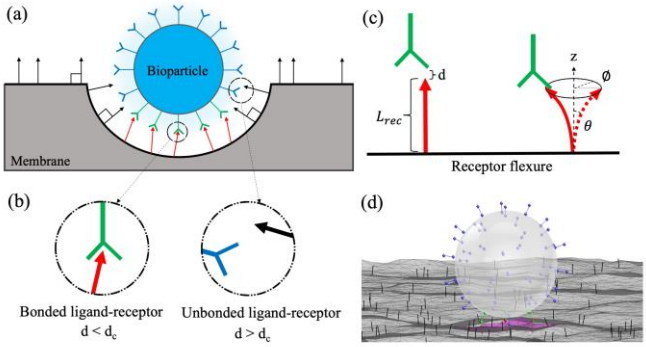

Fig. 2 The binding of particle with the membrane surface. **(a)** Schematic of the binding. The unbonded receptors (black arrow) can freely move on the global cell surface and are assumed to be perpendicular to the local cell surface. **(b)** L_{rec} is the receptor length and d is the tip distance between ligand and receptor. If ligand-receptor tips are within the cutoff range ($d < d_c$), a bond is formed (red-green pair) and no bond is formed (black-blue pair) for $d > d_c$. **(c)** The bonded receptors (red arrows) can bend and rotate in θ and Ø which is a measure for the flexural rigidity, EI. **(d)** A snapshot derived from the beginning of the simulations. Here, unbonded receptors are denoted with black, bonded receptors with red, unbonded ligands with blue and bonded ligands with green, the pink color denotes the area with clathrin on the membrane. This color code is maintained for all the equilibrium profiles shown in this work.

The interactions between the particle and cell membrane occur through the specific interactions between the ligands on the particle and receptors on the cell surface. The particle is modeled as a rigid sphere, coated with ligands that bind specifically to the receptors on the cell surface. The ligands and receptors are coarse-grained as cylinders with one end attached to the particle or membrane surface and the other free end as the binding tip. The length and radius of the ligand/receptor have been chosen to mimic their real dimensions according to the crystal structures.[34,35] The ligands are uniformly coated and fixed at their positions on the particle. The particle is allowed to translate and rotate in random directions. The receptors are placed normal to the local cell surface and can freely move around on the membrane. This model has been rigorously validated in our previous works.[31–33] Schematics of the particle binding to the membrane via ligand-receptor interactions is provided in **Fig. 2 (a)**.

Membrane model

A square patch of elastic membrane is discretized into triangular meshes consisting of vertices, links, and triangles. The free energy of membrane deformation is modeled through Helfrich Hamiltonian.[36] The total energy E of the membrane is expressed as:

$$E = \iint \left[\frac{\kappa}{2}(2H - H_0)^2 + \bar{\kappa}K + \sigma\right] dA \qquad (1)$$

where κ and $\bar{\kappa}$ are the bending rigidity and Gaussian rigidity of the membrane. $H = (c_1 + c_2)/2$ is the mean curvature and $K = c_1 c_2$ is the Gaussian curvature of the surface, where c_1 and c_2 are the principal radii of curvature. H_0 is the intrinsic or spontaneous mean curvature of the membrane. The membrane topology is assumed to be fixed. Thus, the Gaussian term remains a constant and is hence not included in our model. σ is the membrane characteristic tension. Details regarding the membrane model can be found in Ref.[37]. Periodic boundary conditions are applied to the membrane boundaries.

Ligand-receptor interactions

As shown in **Fig. 2(b)**, the ligand-receptor interactions are modeled through the Bell spring model:[38]

$$\Delta G_r(d) = \Delta G_0 + \frac{1}{2}kd^2 \qquad (2)$$

where d is the distance between the binding tips of the interacting ligand-receptor, ΔG_0 is the equilibrium free energy change at $d = 0$, and k is the interaction bond force constant. For binding, the ligand-receptor tip distance, d must be within the reaction cutoff distance, d_c. If the tip distance is beyond this range, no bond will form, and an existing bond may break. Although d_c is an important parameter can be estimated from atomic force microscopic measurement of ligand-receptor interactions , a wide range of values are often used in computational models.[23,26] In our model, we set the the reaction cutoff at ~ $0.9\,nm$ based on the experimental measurement of Tf-TfR interactions.[39]

The flexural movement of the receptors is another crucial component for ligand-receptor interactions since it is directly related to the entropy change during binding. For the receptor flexural movement, as illustrated in **Fig. 2(c)**, we allow the receptors to bend and rotate relative to the local normal direction. Under the assumption of small flexural deformations, we can model the flexure of a receptor as bending of a beam from equilibrium (normal to the cell surface) position, and the bending energy due to flexure can be calculated as:

$$\Delta G_f(\theta) = (2EI/L_{rec})\theta^2 \qquad (3)$$

where EI is the receptor flexural rigidity, L_{rec} is the receptor length and θ represents the bending angle from the normal axis of the local triangle. Due to the complexity of capturing such mechanical property at a nanoscale level, reliable techniques for measuring receptor flexural rigidity are limited. Since the EI for TfR has not been experimentally reported in the literature, in our model EI was set at $7000\,pN.nm^2$. This value was chosen between that of glycoproteins ($700\,pN.nm^2$) and actin filament ($15 - 73 \times 10^3\,pN.nm^2$).[40] The binding energy change for each ligand-receptor interaction is the difference between the energy reduction by ligand-receptor interaction and the energy increase through receptor bending.

Clathrin model

The effects of clathrin on the membrane are treated as additional intrinsic curvature and modified bending rigidity, and then the total energy of the system with clathrin is calculated as:

$$E = \iint \left[\frac{\kappa}{2}(2H)^2 + \sigma\right] dA + \iint \left[\frac{\kappa_{cla}}{2}(2H - H_{cla})^2\right] dA \quad (4)$$

The first term accounts for the regions without clathrin and the second term represents the effects from regions with clathrin. κ_{cla} and H_{cla} are the bending rigidity and intrinsic curvature of the clathrin coat, respectively. The recruitment of the clathrin is modeled as a ligand-receptor dependent process. Each time when a new bond between ligand-receptor is formed, clathrin accumulates at that new binding site. The impact from clathrin is represented by the curvature field. The intrinsic curvature, H_{cla}, is applied to the vertices within an area, and the radius ($14\ nm$) of the area is determined by the clathrin polygon detected from experiments. [41] The local clathrin will disappear only if the nanoparticle completely detaches from the membrane surface. Details of the clathrin model can be found in our previous work.[31–33]

Monte Carlo simulation

As shown in **Fig. 2(d)**, our system contains four Monte Carlo types of movements: receptor diffusion, particle translation or rotation, ligand-receptor interaction, and membrane surface evolution. During receptor diffusion and particle translation/rotation, the membrane topology is fixed. The free receptors always move on the membrane surface and are pointed to the normal direction of the local surface. When the particle is translated or rotated, the ligands are translated or rotated along with the particle. The particle translation or rotation may cause the reaction energy change or even breakage of bonds between ligands and receptors. If the distance between the tips of the bonded ligand and receptor is greater than the reaction cutoff d_c after the movement, this bond breaks and the receptor tip position is reset to be perpendicular to its local triangle. In each Monte Carlo step, one of the movements from above will be randomly selected and the system energy (U) for the new configuration (U_{new} contains contributions from membrane elastic energy E (Eq. (1) or (4)), ligand-receptor reaction energy ΔG_r (Eq. (2)) and the receptor flexural energy ΔG_f (Eq. (3))) will be calculated, and then the new configuration will be accepted with the following probability: $min\{1, exp\ [-(U_{new} - U_{old})/k_BT]\}$, where k_B is the Boltzmann constant and T is the system temperature. The ligand-receptor bond formation/breakage is considered to be stochastic process. Within a reaction distance, a ligand-receptor pair is randomly selected and if they are unbonded, the bond may form with a probability: $min\{1, exp[-\Delta G/k_BT]\}$. If the pair is already bonded, the bond may break with a probability: $min\{1, exp[\Delta G/k_BT]\}$, where ΔG is the energy change due to the bond formation/breakage calculated from Eqs. (2) and (3).

Results and discussions

Effects of receptor flexural rigidity on CME

Bending of the receptors may have profound impacts on the ligand-receptor bond formation/breakage and the internalization of particles. Most of the existing models have not considered this effect. Here, through our model we first investigate the effect of receptor flexural rigidity on clathrin dependent RME.

Throughout this work, parameters from transferrin receptor (TfR) and its corresponding ligand (Tf) have been used. For simulation setup, the particle radius was fixed at $40\ nm$ with 106 ligands on its surface, the receptor length was fixed at $9.3\ nm$ and reaction cutoff distance at $0.9\ nm$. The flexural rigidity EI was varied from 20000 to $45000\ pN.nm^2$. These values lie in between the EI values for glycoproteins ($700\ pN.nm^2$) and actin filaments ($15 - 73 \times 10^3\ pN.nm^2$). All other parameters were kept fixed as provided in **Table 1** in Appendix. Five independent simulations were performed for each value of EI to ensure the statistical consistency (**Fig. S1** in ***ESI*** shows the results from all 5 independent realizations for

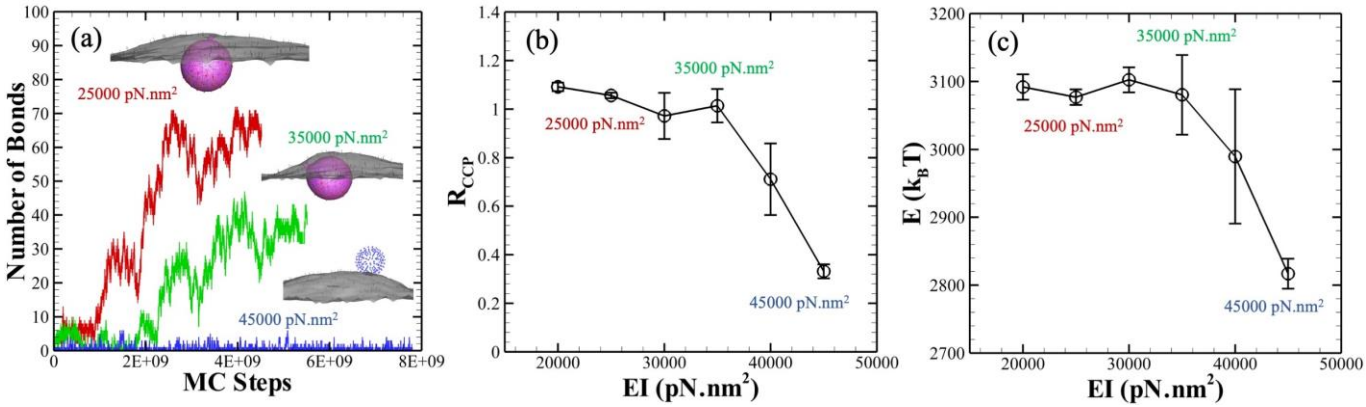

Fig. 3 Receptor flexural rigidity effects on clathrin-dependent RME. **(a)** The number of bonds and the equilibrium profiles for three EI values. Although for both the red and green cases the particle is fully internalized, the latter one forms lesser number of bonds. **(b)** The CCP area ratio at different receptor rigidities. A value around 1 indicates that the particle has fully internalized. **(c)** Membrane deformation energy at equilibrium at different receptor rigidities. Complete particle wrapping requires high degree of membrane deformation which correlates to the high deformation energy. The error bars in **(b)** and **(c)** are calculated based on five independent simulations.

$EI = 20000\ pN.nm^2$). To quantify the stages of particle internalization, we define R_{CCP} as the ratio of the clathrin coated pit (CCP) area to the minimum area required to encapsulate the particle; $R_{CCP} > 1$ means the particle has fully internalized with a visible neck region. As shown in **Fig. 3(b)**, when the flexural rigidity is increased, the value of R_{CCP} decreases from 1, indicating that the particle will not be completely internalized at very high values of EI. This demonstrates an inverse relationship between the EI and the particle encapsulation. Interestingly, the error bars in Fig. 3(b) are significantly larger in the range between $30{,}000$ and $40{,}000\ pN.nm^2$, indicating a transition region in which the particle internalization dramatically changes among different realizations (see **Fig. S2** in ***ESI***). To show these effects in more detail, three values of EI (25000, 35000 and $45000\ pN.nm^2$) have been selected and their number of bonds with MC steps as well as their equilibrium profiles are presented in **Fig. 3(a)**. It is evident, that for lower value of EI (red line), the number of bond formations is very high and much faster (in terms of MC steps) than the higher values of EI (green line). For the highest EI value (blue line), there is no particle internalization, and the particle just moves on top of the membrane experiencing continuous breakage and formation of bonds. Even though both red and green cases achieve complete internalization, the number of bonds formed during the internalization is much less when EI is higher. Internalization with lower number of bonds may not be a concern for endocytosis, however, it can be desirable for exocytosis since it will facilitate faster expulsion.

The free energy of membrane deformation (Eq. (4)) at equilibrium is also useful to characterize particle internalization. In **Fig. 3(c)**, the mean deformation energy (averaged over the final 100 million MC steps) is presented for each EI. Consistent with **Fig. 3(b)**, stiffer receptors with $EI > 35000\ pN.Nm^2$ obstruct bond formations with ligands, which leads to insufficient membrane deformation and partial to no wrapping as observed from the energy profile.

The above results suggest that the receptor flexural rigidity plays important roles during the endocytosis process and there exists a threshold beyond which particle encapsulation will not occur. This is reasonable since larger EI value corresponds to a stiffer receptor which exhibits high resistance against bending. But for ligand-receptor interactions, less stiffness is desirable which can facilitate formation of more bonds and promotes faster endocytosis.

Effect of receptor length, L_{rec}, on endocytosis

In this section, we investigate the impacts of one of the geometrical parameters, receptor length $\boldsymbol{L_{rec}}$, on endocytosis for both with and without clathrin cases. The reaction cutoff distance, $\boldsymbol{d_c}$, between the ligand and receptor has been kept constant at $\boldsymbol{0.9\ nm}$. The other parameters are provided in **Table 1** in Appendix. Since our focus here is only on the receptor length, the receptor radius and the length and radius of the ligands have been kept constant. The crystal structures of different types of receptors have been reported in the literature.[35,42–46] By fitting the crystal structure data, we can estimate the receptor length ranging from $\sim \boldsymbol{2\ nm}$ to $\sim \boldsymbol{10\ nm}$. For instance, the length of low density lipoprotein (LDL) receptor which is involved in RME of LDL/cholesterol was estimated to be $\sim \boldsymbol{3\ nm}$ from its crystal structure.[46] Therefore, we start with the value of $\boldsymbol{9.3\ nm}$ which is the estimated length for TfR[35] and gradually reduce it to half in several steps. So, the chosen values for $\boldsymbol{L_{rec}}$ are $\boldsymbol{9.3, 4.6, 2.3, 1.2, 0.6}$ and $\boldsymbol{0.3\ nm}$. Three independent simulations have been conducted for each case to ensure statistical consistency (**Fig. S3** in ***ESI*** show the results from all three independent realizations for the case of $\boldsymbol{L_{rec} = 2.3\ nm}$).

As shown in **Fig. 4(a)**, with clathrin we see full endocytosis of the bioparticle for all the cases since the clathrin is the principal driving force for particle internalization. As illustrated for three of these cases (for receptor length of $\boldsymbol{9.3, 2.3}$ and $\boldsymbol{0.6\ nm}$), the number of bonds reaches a very high value for all of them. Their equilibrium profiles show the full internalization where the pink color denotes the clathrin-coated pit. The number of available ligands on the particle surface was kept constant at $\boldsymbol{162}$ for all cases and we see the number of bonds can be as high as $\sim\boldsymbol{155}$. An interesting observation is that the number of bonds experiences two rapid increase for complete particle internalization, which correspond to the wrapping process of the bottom and top half of the particle respectively. To demonstrate the effects from clathrin, we keep all the parameters the same and remove the clathrin from our model. **Fig. 4(b)** shows the equilibrium profiles and the number of bonds for

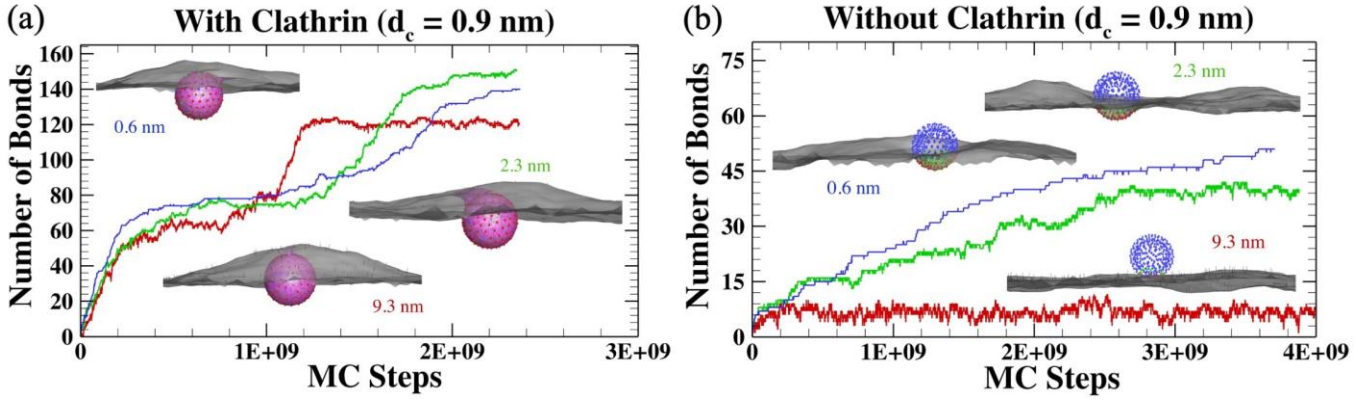

Fig. 4 Effect of receptor length, L_{rec}. The number of bonds and equilibrium profiles for $L_{rec} = 9.3, 2.3\ and\ 0.6\ nm$ in case of **(a)** clathrin-dependent RME (particles are fully internalized and the pink region denotes the clathrin-coated pit) and **(b)** clathrin-independent RME (particles are only partially internalized for all cases).

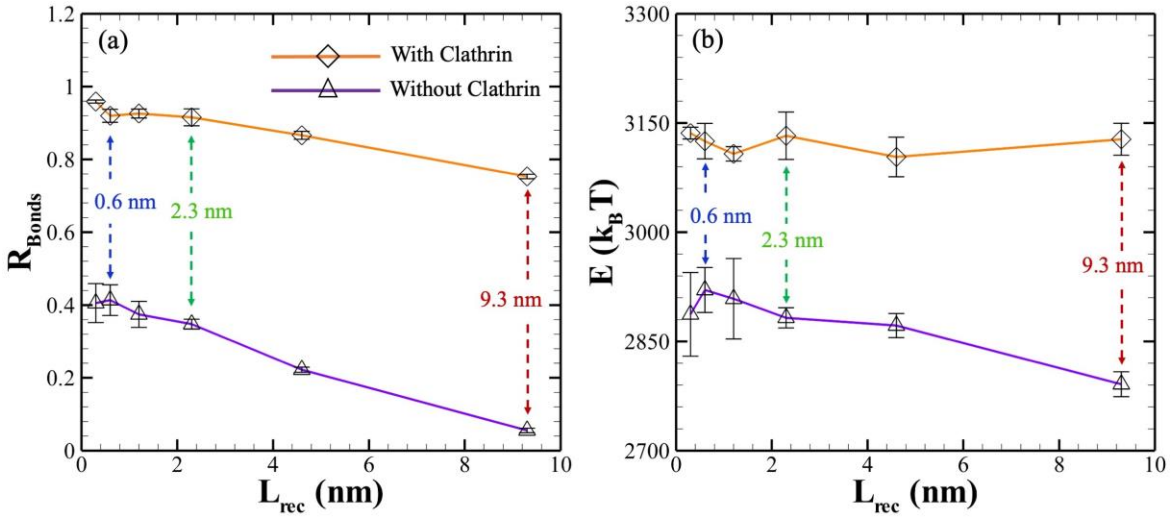

Fig. 5 (a) The ratio of bonded ligands to total available ligands (R_{Bonds}), for both clathrin-dependent (orange) and clathrin-independent (purple) RME at different receptor lengths. It is evident that a smaller number of bonds are formed for longer receptors. **(b)** Membrane deformation energy for different receptor lengths. Energy profiles for both with and with clathrin cases are provided. The error bars are calculated based on three independent simulations.

the same receptor lengths ($\mathbf{9.3}, \mathbf{2.3}$ and $\mathbf{0.6}\ \boldsymbol{nm}$, given by the red, green, and blue color respectively) for without-clathrin case. It is evident that the number of bonds for $\boldsymbol{L_{rec} = 9.3\ nm}$ is very low. As we decrease receptor length, the number bonds keep increasing. Despite a rise in the number of bonds, we do not observe complete internalization for all three cases. The particles are only partially internalized with shorter $\boldsymbol{L_{rec}}$.

To quantify the number of formed bonds during internalization, we define R_{Bonds} as the ratio between the number of bonds at equilibrium and the total number of available ligands on the particle surface ($e.g. 162$). As shown in **Fig. 5(a)**, with clathrin R_{Bonds} starts at around ~ 0.7 and goes as high as ~ 0.95 as the receptor length decreases. Similar trend is also observed in cases without clathrin but with much lower number of bonds. This indicates that the shorter receptor lengths facilitate the formation of ligand-receptor bonds. The energy of membrane deformation at different receptor lengths is provided in **Fig. 5(b)**, for both with and without clathrin cases. In presence of clathrin, the clathrin becomes the dominant factor and drives all particles to complete internalization irrespective of the receptor length. That is why similar deformation energy is observed for all receptor lengths (orange line). In absence of clathrin, the membrane deformation is insufficient, as denoted by the lower free energy of deformation for all cases (purple line). However, an effect of the receptor length is observed as the membrane deformation energy as well as particle wrapping is reduced for longer receptors.

These findings suggest that it is important to consider the physical length of the receptors in a numerical model. However, most of the existing models[27–30,47,48] have simplified the receptors as spherical beads, and may lead to unrealistic particle internalization.

Effect of reaction cutoff, d_c, on endocytosis

The reaction cutoff is another crucial parameter for numerical models of endocytosis. To form bonds between the ligands on the particle and the corresponding receptors on the cell surface, their free tips have to be within the reaction cutoff. In this section, we setup our simulations to systematically investigate the impacts of reaction cutoff on endocytosis. Since the particles will always be internalized with the existence of clathrin within our parameter range, here we only present the cases without clathrin.

For our simulations, the reaction cutoff distance has been varied from $d_c = 0.9\ nm$ which was used in our previous studies. We have selected five more values with an increment of $1\ nm$ from the initial value to have $d_c = 1.9, 2.9, 3.9, 4.9$ and $5.9\ nm$. We also choose two different values of receptor length, $L_{rec} = 9.3$ and $0.3\ nm$, to show the combined effects of receptor length and reaction cutoff. In **Fig. 6(a)**, the number of bonds and equilibrium profiles for three of the cutoffs ($1.9, 3.9\ and\ 5.9\ nm$, given by the red, green, and blue color respectively) are shown where the receptor length is fixed at $9.3\ nm$. As expected, the number of bonds increases gradually with increasing reaction cutoff. However, we do not observe complete internalizations for all the cases. As demonstrated from the equilibrium profiles, there is a gradual increase in the expanse of partial wrapping as the reaction cutoff is increased, but there is no full wrapping of the nanoparticle.

Interestingly, when we reduce the receptor length to $0.3\ nm$, results are quite different as shown in **Fig. 6(b)**. As d_c is increased, the number of bonds gradually increases and reaches a very high value, as high as ~ 160 (blue line in **Fig. 6(b)**), for the

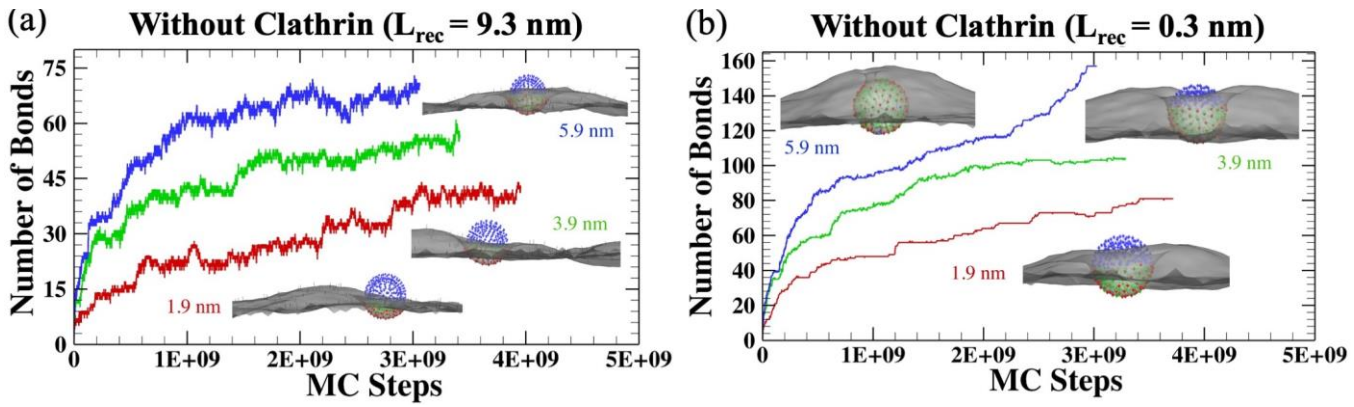

Fig. 6 Effect of reaction cutoff, d_c, on RME without clathrin. **(a)** The number of bonds and equilibrium profiles for $d_c = 1.9, 3.9$ and $5.9\ nm$ for receptor length of $L_{rec} = 9.3\ nm$. Particles are only partially wrapped for all cases though there is a gradual increase in number of bonds with higher cutoff. **(b)** The number of bonds and equilibrium profiles are given for same d_c values but with the lowest receptor length, $L_{rec} = 0.3\ nm$. It's evident that the membrane wrapping around the particle is higher and the particle gets fully wrapped at $d_c = 5.9\ nm$.

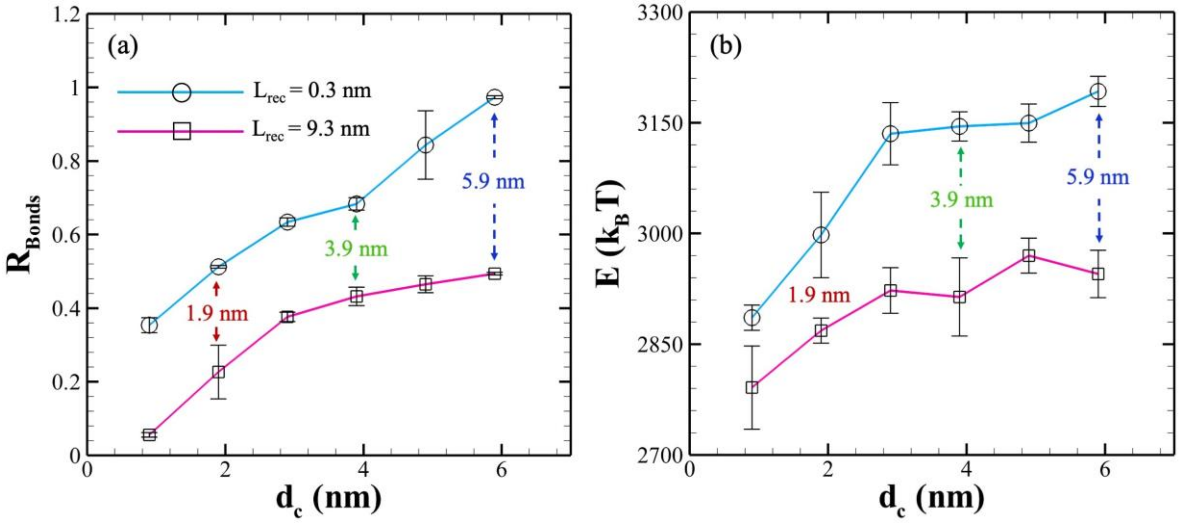

Fig. 7 (a) The ratio of bonded ligands to total available ligands (R_{Bonds}) at different reaction cutoffs, for both long receptor ($L_{rec} = 9.3\ nm$) and short receptor ($L_{rec} = 0.3\ nm$). **(b)** Membrane deformation energy for different reaction cutoffs. For both receptor lengths, reaction cutoff effect is clearly observed. Larger reaction cutoff facilitates greater deformation. The error bars are calculated based on three independent simulations.

cutoff $d_c = 5.9\ nm$. And it is clear that the particle is completely internalized. **Figure 7 (a)** summarizes the effects of reaction cutoff by looking at the ratio of the number of bonds (R_{Bonds}) for both receptor lengths. In general, as the reaction cutoff is increased, the number of formed bonds increases. But at the higher receptor length, particles are only partially internalized as reflected from $R_{Bonds} < 0.5$. As the receptor length is reduced to $0.3\ nm$, a complete internalization can be achieved at higher reaction cutoff ($R_{Bonds} \sim 1$). **Fig. 7(b)** shows the energy profiles of membrane deformation for both receptor lengths. The effect of reaction cutoff is quite clear, larger reaction cutoff leads to higher deformation energy. However, the energy profile for shorter receptor is always higher than the longer receptor at the same reaction cutoff. This also confirms that the shorter receptor length, with large reaction cutoff, facilitates greater membrane deformation and eventually leads to complete particle internalization.

These results demonstrate that both receptor length and ligand-receptor reaction cutoff play critical roles for a successful particle internalization in numerical models.

Conclusions

In this paper, we implemented a Monte Carlo based stochastic model to study the internalization of ligand-coated nanoparticles via receptor mediated endocytosis. We systematically investigated the effects of a wide range of mechanical parameters (receptor flexural rigidity, EI), geometrical parameters (receptor length, L_{rec}) and biochemical parameters (ligand-receptor reaction cutoff, d_c),

on particle internalization both individually and collectively, with and without the presence of clathrin.

The results from our simulations showed that the receptor flexural rigidity played important roles in clathrin-mediated endocytosis. There is a threshold of EI beyond which particle internalization will not occur. For ligand-receptor interactions, smaller EI is desirable which can facilitate formation of more ligand-receptor bonds and promotes faster internalization. Also, our results indicated that the clathrin is the primary driving force for particle internalization. Without clathrin, a complete endocytosis is very unlikely through ligand-receptor interactions only. Shorter receptor length and longer ligand-receptor reaction cutoff promote formation of ligand-receptor bonds and facilitate particle internalization. But we showed through our simulations that without clathrin, particles can only be partially internalized in most of the cases. In absence of clathrin, a complete internalization can only be obtained through ligand-receptor interactions with extremely short receptor length and long reaction cutoff. Considering the complexity of the receptor mediated endocytosis and recent discovery of different clathrin-independent endocytosis processes, one needs to be cautious when correlating the results from clathrin-free simulations with experimental observations. It is highly possible that there exist some other driving mechanisms, in addition to ligand-receptor interactions, for membrane deformation and particle internalization. Our model is flexible and can be readily extended to incorporate such mechanisms in a similar way as clathrin.

Appendix A: Simulation parameters

The **Table 1** below lists some of the simulation parameters used and the corresponding references:

Parameter	Value	Ref
Size of the membrane surface	$910\ nm \times 910\ nm$	
Membrane bending rigidity, κ_m	$20\ k_BT$	49
Membrane characteristic tension, σ	$0.001\ pNnm^{-1}$	22
Clathrin bending rigidity, κ_{cla}	$200\ k_BT$	50
Clathrin intrinsic curvature, H_{cla}	$0.036\ nm^{-1}$	51
Nanocarrier diameter	$35\ nm$	
Ligand length	$9\ nm$	34
Ligand radius	$2.5\ nm$	34
Receptor length, L_{rec}	$9.3\ to\ 0.3\ nm$	
Receptor radius	$5\ nm$	35
Number of ligands on particle	162	52
Number of receptors on the cell	300	53
Equilibrium free energy change, ΔG_0	$-8.64e^{-20}J$	39
Reaction cutoff, d_c	$0.9\ to\ 5.9\ nm$	
Receptor flexural rigidity, EI	$20000 - 45000\ pN.nm^2$	40
System temperature	$298\ K$	

Conflicts of interest

There are no conflicts to declare.

Acknowledgements

This work used Expanse CPU at SDSC through allocation MCB170012 from the Advanced Cyberinfrastructure Coordination Ecosystem: Services & Support (ACCESS) program, which is supported by National Science Foundation grants #2138259, #2138286, #2138307, #2137603, and #2138296.

References

1 J. Grove and M. Marsh, *J. Cell Biol.*, 2011, **195**, 1071–1082.
2 M. Marsh and A. Helenius, *Cell*, 2006, **124**, 729–740.
3 J. Mercer, M. Schelhaas and A. Helenius, *Annu. Rev. Biochem. Vol 79*, 2010, **79**, 803–833.
4 D. K. Bonner, C. Leung, J. Chen-Liang, L. Chingozha, R. Langer and P. T. Hammond, *Bioconjug. Chem.*, 2011, **22**, 1519–1525.
5 J. Y. Han, B. J. Zern, V. V. Shuvaev, P. F. Davies, S. Muro and V. Muzykantov, *Acs Nano*, 2012, **6**, 8824–8836.
6 D. Peer, J. M. Karp, S. Hong, O. C. FaroKHzad, R. Margalit and R. Langer, *Nat. Nanotechnol.*, 2007, **2**, 751–760.
7 L. Hinrichsen, A. Meyerhoiz, S. Groos and E. J. Ungewickell, *Proc. Natl. Acad. Sci. U. S. A.*, 2006, **103**, 8715–8720.
8 P. N. Dannhauser and E. J. Ungewickell, *Nat. Cell Biol.*, 2012, **14**, 634-+.
9 R. Nossal, *Traffic*, 2001, **2**, 138–147.
10 S. J. Royle, *Cell. Mol. Life Sci.*, 2006, **63**, 1823–1832.
11 J. X. Chen, J. Z. Wang, K. R. Meyers and C. A. Enns, *Traffic*, 2009, **10**, 1488–1501.
12 J. Schlessinger, *Cell*, 2000, **103**, 211–225.
13 S. B. Sieczkarski and G. R. Whittaker, *J. Virol.*, 2002, **76**, 10455–10464.
14 M. Lakadamyali, M. J. Rust and X. Zhuang, *Microbes Infect.*, 2004, **6**, 929–936.
15 J. Voigt, J. Christensen and V. P. Shastri, *Proc. Natl. Acad. Sci.*, 2014, **111**, 2942–2947.
16 M. Chatterjee, E. Ben-Josef, R. Robb, M. Vedaie, S. Seum, K. Thirumoorthy, K. Palanichamy, M. Harbrecht, A. Chakravarti and T. M. Williams, *Cancer Res.*, 2017, **77**, 5925–5937.
17 H. F. Renard and E. Boucrot, *Curr. Opin. Cell Biol.*, 2021, **71**, 120–129.
18 M. S. de Almeida, E. Susnik, B. Drasler, P. Taladriz-Blanco, A. Petri-Fink and B. Rothen-Rutishauser, *Chem. Soc. Rev.*, 2021, **50**, 5397–5434.
19 D. Gonzalez-Rodriguez and A. I. Barakat, *PLOS ONE*, 2015, **10**, e0122097.
20 T. Zhang, R. Sknepnek, M. J. Bowick and J. M. Schwarz, *Biophys. J.*, 2015, **108**, 508–519.
21 D. M. Richards and R. G. Endres, *Proc. Natl. Acad. Sci.*, 2016, **113**, 6113–6118.
22 J. E. Hassinger, G. Oster, D. G. Drubin and P. Rangamani, *Proc. Natl. Acad. Sci.*, 2017, **114**, E1118–E1127.
23 C. Huang, Y. Zhang, H. Yuan, H. Gao and S. Zhang, *Nano Lett.*, 2013, **13**, 4546–4550.
24 S. Dasgupta, T. Auth and G. Gompper, *Nano Lett.*, 2014, **14**, 687–693.
25 Z. Shen, H. Ye and Y. Li, *Phys. Chem. Chem. Phys.*, 2018, **20**, 16372–16385.

26 Z. Q. Shen, H. L. Ye, X. Yi and Y. Li, *Acs Nano*, 2019, **13**, 215–228.
27 R. Vacha, F. J. Martinez-Veracoechea and D. Frenkel, *Nano Lett.*, 2011, **11**, 5391–5395.
28 H. M. Ding and Y. Q. Ma, *Biomaterials*, 2012, **33**, 5798–5802.
29 Y. Li, T. T. Yue, K. Yang and X. R. Zhang, *Biomaterials*, 2012, **33**, 4965–4973.
30 T. T. Yue and X. R. Zhang, *Soft Matter*, 2013, **9**, 559–569.
31 H. Deng, P. Dutta and J. Liu, *Biochim. Biophys. Acta-Gen. Subj.*, 2018, **1862**, 2104–2111.
32 H. Deng, P. Dutta and J. Liu, *Nanoscale*, 2019, **11**, 11227–11235.
33 H. Deng, P. Dutta and J. Liu, *Soft Matter*, 2019, **15**, 5128–5137.
34 H. M. Berman, J. Westbrook, Z. Feng, G. Gilliland, T. N. Bhat, H. Weissig, I. N. Shindyalov and P. E. Bourne, *Nucleic Acids Res.*, 2000, **28**, 235–242.
35 H. Fuchs, U. Lücken, R. Tauber, A. Engel and R. Gessner, *Struct. Lond. Engl. 1993*, 1998, **6**, 1235–1243.
36 W. Helfrich, *Z Naturforsch*, 1973, **C 28**, 693-703.
37 N. Ramakrishnan, P. B. Sunil Kumar and J. H. Ipsen, *Phys. Rev. E Stat. Nonlin. Soft Matter Phys.*, 2010, **81**, 041922.
38 G. I. Bell, M. Dembo and P. Bongrand, *Biophys. J.*, 1984, **45**, 1051–1064.
39 A. Yersin, T. Osada and A. Ikai, *Biophys. J.*, 2008, **94**, 230–240.
40 S. Weinbaum, X. B. Zhang, Y. F. Han, H. Vink and S. C. Cowin, *Proc. Natl. Acad. Sci. U. S. A.*, 2003, **100**, 7988–7995.
41 J. Heuser and T. Kirchhausen, *J. Ultrastruct. Res.*, 1985, **92**, 1–27.
42 A. J. Lapthorn, D. C. Harris, A. Littlejohn, J. W. Lustbader, R. E. Canfield, K. J. Machin, F. J. Morgan and N. W. Isaacs, *Nature*, 1994, **369**, 455–461.
43 C. Larsen, A. Etzerodt, M. Madsen, K. Skjødt, S. K. Moestrup and C. B. F. Andersen, *Nat. Commun.*, 2018, **9**, 5204.
44 D. E. Vaughn and P. J. Bjorkman, *Struct. Lond. Engl. 1993*, 1998, **6**, 63–73.
45 G. A. Snyder, A. G. Brooks and P. D. Sun, *Proc. Natl. Acad. Sci. U. S. A.*, 1999, **96**, 3864–3869.
46 W. Huang, K. Dolmer and P. G. Gettins, *J. Biol. Chem.*, 1999, **274**, 14130–14136.
47 X. H. Shi, A. von dem Bussche, R. H. Hurt, A. B. Kane and H. J. Gao, *Nat. Nanotechnol.*, 2011, **6**, 714–719.
48 T. T. Yue and X. R. Zhang, *Soft Matter*, 2011, **7**, 9104–9112.
49 E. Evans and W. Rawicz, *Phys. Rev. Lett.*, 1990, **64**, 2094–2097.
50 A. J. Jin, K. Prasad, P. D. Smith, E. M. Lafer and R. Nossal, *Biophys. J.*, 2006, **90**, 3333–3344.
51 S. Zaremba and J. H. Keen, *J. Cell Biol.*, 1983, **97**, 1339–1347.
52 D. T. Wiley, P. Webster, A. Gale and M. E. Davis, *Proc. Natl. Acad. Sci. U. S. A.*, 2013, **110**, 8662–8667.
53 J. D. Bleil and M. S. Bretscher, *Embo J.*, 1982, **1**, 351–355.